The Young Star Cluster System in the Antennae: Evidence for a Turnover in the luminosity function

P. Anders[1,2]⋆, N. Bissantz[3,4], L. Boysen[4], R. de Grijs[5], and U. Fritze – v. Alvensleben[1,6]

[1] *Institut für Astrophysik, University of Göttingen, Friedrich-Hund-Platz 1, 37077 Göttingen, Germany*
[2] *Sterrenkundig Instituut, Universiteit Utrecht, P.O. Box 80000, 3508 TA Utrecht, The Netherlands*
[3] *Institut für Mathematische Stochastik, University of Göttingen, Maschmühlenweg 8-10, 37073 Göttingen, Germany*
[4] *Fakultät für Mathematik, Ruhr-University of Bochum, Mathematik III, NA 3/70, Universitätsstraße 150, 44780 Bochum, Germany*
[5] *Department of Physics & Astronomy, The University of Sheffield, Hicks Building, Hounsfield Road, Sheffield S3 7RH*
[6] *Centre for Astrophysics Research, University of Hertfordshire, College Lane, Hatfield AL10 9AB*

ABSTRACT

The luminosity functions (LFs) of star cluster systems (i.e. the number of clusters per luminosity interval) are vital diagnostics to probe the conditions of star cluster formation. Early studies have revealed a clear dichotomy between old globular clusters and young clusters, with the former characterised by Gaussian-shaped LFs, and the latter following a power law. Recently, this view was challenged by studies of galaxy merger remnants and post-starburst galaxies. In this paper we re-evaluate the young ($\lesssim$ few hundreds of Myrs, with the majority $\lesssim$ few tens of Myrs) star cluster system in the ongoing spiral-spiral major merger system NGC 4038/39, the "Antennae" galaxies. The Antennae galaxies represent a very active and complex star-forming environment, which hampers cluster selection and photometry as well as the determination of observational completeness fractions. A main issue of concern is the large number of bright young stars contained in most earlier studies, which we carefully exclude from our cluster sample by accurately determining the source sizes. The resulting LFs are fitted both with Gaussian and with power-law distributions, taking into account both the observational completeness fractions and photometric errors, and compared using a likelihood ratio test. The likelihood ratio results are rigidly evaluated using Monte Carlo simulations. We perform a number of additional tests, e.g. with subsets of the total sample, all confirming our main result: that a Gaussian distribution fits the observed LFs of clusters in this preferentially very young cluster system significantly better than a power-law distribution, at a (statistical) error probability of less than 0.5 per cent.

Key words: globular clusters: general – open clusters and associations: general – galaxies: star clusters – galaxies: evolution – methods: data analysis

1 INTRODUCTION

1.1 Star Clusters: evolution and interpretation

Star clusters (SCs) form nearly instantaneously through the collapse of giant molecular gas clouds (GMCs). Hence all stars within a SC are approximately coeval, and represent a simple stellar population (SSP). A small number of parameters, in particular their initial chemical composition and initial stellar mass function (IMF), are enough to describe their colour and luminosity evolution on the basis of

a given set of stellar evolutionary tracks or isochrones (e.g. Schulz et al. 2002, Anders & Fritze-v. Alvensleben 2003, Bruzual & Charlot 2003). Therefore, observed spectrophotometric properties of SCs are relatively easy and straightforward to interpret.

SC formation is a major mode of all star formation, and possibly even the dominant mode in strong starbursts triggered in gas-rich galaxy mergers (e.g., Meurer 1995, de Grijs et al. 003a).

SCs are excellent tracers of their parent galaxy's starforming properties. Radial age gradients in SC systems and age differences between SF regions tell us about the dynam-

⋆ E-mail: P.Anders@astro.uu.nl

ical evolution of a starburst (de Grijs et al. 2001). This is owing to the fact that SCs are not only relatively easy to model but also much easier to analyse than the integrated light of the galaxy, because SCs can be studied individually. Even without individual SC spectroscopy, multi-band imaging in at least four suitable passbands allows us to determine the age, metallicity, extinction, and mass of a SC (Anders et al. 004a,b). The age and metallicity distributions of a SC system directly reveal the SF and chemical enrichment histories of its parent galaxy, to much higher precision than studies of the galaxy's integrated light, since the latter is always dominated by the last major epoch of SF (see e.g. Fritze-v. Alvensleben 2004). The long-lived SCs, and the old globular clusters (GCs) in particular, hold a key role in this respect (cf. West et al. 2004).

1.2 Star Cluster Systems

The most commonly used diagnostics to explore the properties and evolution of entire SC *systems* are their luminosity and mass functions[1] (LFs, MFs).

For old GC systems in the local Universe, both LFs and MFs are of log-normal ("Gaussian") shape, with very similar parameters among a wide variety of galaxies (Ashman & Zepf 1998, Harris 1991; minor trends with metal content can easily be accounted for, cf. Ashman et al. 1995), with a Gaussian peak (or "turnover") magnitude at $M_V = -7.3$ mag and a Gaussian FWHM of 2.8 mag, corresponding to a Gaussian $\sigma = 1.2$ mag. This universal turnover of GC LFs is often used as "secondary" long-range extragalactic distance indicator, and hence for determinations of the Hubble constant and, as a consequence, of the expansion rate of the Universe (Sandage & Tammann 1995, Forbes 1996, Kavelaars et al. 2000).

Young star clusters (YSCs, often referred to as "open" or "populous" clusters) in the local Universe seem to be of a different character than the ubiquitous GCs. In the Milky Way, young clusters are mainly sparse, low-mass objects ($\sim 10^3 - 10^4$ M$_\odot$), with low concentration and lifetimes of order 10^8 yr, that will soon dissolve into the field star population. The Galactic open cluster compilation of van den Bergh & Lafontaine (1984) suggests a LF of power law-type with slope $\alpha \lesssim 0.5$ (but it might be steeper due to incompleteness effects). The only local galaxies with a large number of young clusters with masses $\gtrsim 10^4$ M$_\odot$ (up to masses $\lesssim 3 \times 10^5$ M$_\odot$) are the Magellanic Clouds. Work by Elson & Fall (1985), Elmegreen & Efremov (1997) and Hunter et al. (2003) suggested a luminosity spectrum with a power law of the form $N_{\rm YSC}(L){\rm d}L \propto L^\alpha {\rm d}L$, where $N_{\rm YSC}(L){\rm d}L$ is the number of young star clusters (YSCs)

with luminosities between L and $L + {\rm d}L$, with $\alpha \approx -2$ (corresponding to a LF with $\alpha \approx -1$). Recently, this power-law result was challenged by de Grijs & Anders (2006), who find significant deviations from a power law for clusters in the Large Magellanic Cloud (LMC) of ages younger than $\simeq 100$ Myr and masses below $\simeq 3 \times 10^3$ M$_\odot$.

Rich systems of YSCs are routinely observed in starburst galaxies, in particular in strong starbursts triggered by gas-rich galaxy interactions and mergers (e.g., Whitmore et al. 1993, Schweizer & Seitzer 1998, Zepf et al. 1999, Zhang et al. 2001, de Grijs et al. 2001, 003a,b). Merger remnants with post-starburst signatures also reveal SC systems with ages of up to 1–3 Gyr (e.g., de Grijs et al. 003c, Goudfrooij et al. 2004), indicating that at least some fraction of the SCs formed during a merger-induced burst survived much longer than most of the open clusters in the Milky Way. The LFs of these YSC systems are usually adopted to be of power law-type (see e.g. de Grijs et al. 003b for a recent compilation), but see Fritze-v. Alvensleben (1998, 1999), as well as de Grijs et al. (003c) and Goudfrooij et al. (2004) for Gaussian-shaped LFs of young and intermediate-age cluster systems, respectively.

The lower maximum masses of the YSCs in the Milky Way as compared to YSCs in the LMC and in starburst/merging galaxies could be (partially) understood by the (purely statistical) size-of-sample effect, studied e.g. by Hunter et al. (2003): In the latter galaxies the total number of YSCs is larger than in the Milky Way, therefore the MFs are sampled up to higher masses.

It has hitherto remained unclear whether the difference in shape between the power-law LFs of young SCs (but see Fritze-v. Alvensleben 1998, 1999, Cresci et al. 2005, de Grijs et al. 003c and Goudfrooij et al. 2004 for the Gaussian LFs in the Antennae galaxies [all clusters], NGC 5253 [clusters older than 10 Myr], M82B [contains clusters at roughly 1 Gyr] and NGC 1316 [contains clusters at roughly 3 Gyr], and the new results by de Grijs & Anders 2006 on the LMC SC system) and old GC systems is caused by differences in the nature and formation of the two types of clusters, or whether the power law of young systems is secularly transformed into the Gaussian distribution of old GC systems by selective destruction effects.

1.3 Our case study: the Antennae system

In this paper we study the YSC system of the Antennae galaxies (NGC 4038/39), the best-studied and nearest example of a major interaction between two massive gas-rich spiral galaxies, at a distance of 19.2 Mpc [2]. In addition, the low inclination of both galaxies favours the detection and study of their SC systems. In the Antennae galaxies, both the individual SCs (see e.g. Whitmore & Schweizer 1995, Fritze-v. Alvensleben 1998, 1999, Zhang et al. 2001,

---

[1] Following McLaughlin & Pudritz (1996) and Parmentier & Gilmore (2006) we denote a luminosity *spectrum* (LS) the number of objects per *linear* luminosity interval ${\rm d}N/{\rm d}L$, while we refer to the luminosity *function* (LF) to describe the number of objects per *logarithmic* interval ${\rm d}N/{\rm d}\log L$. Magnitudes (mag) are logarithmically related to luminosities (L) $\log L \propto mag$. If a LS can be described by a power law $L^{-\alpha_{LS}}$, the slope of the corresponding LF is $\alpha_{LF} = \alpha_{LS} - 1$ and if expressed in magnitudes $\alpha_{LF'} = 0.4 \times (\alpha_{LS} - 1) = 0.4 \times \alpha_{LF}$. In this paper we discuss LFs expressed in magnitudes. Mass *functions* are defined similarly.

[2] Throughout this paper we adopt a distance to the Antennae galaxies of 19.2 Mpc ($m - M = 31.4$ mag; see e.g. Whitmore & Zhang 2002, Kassin et al. 2003, Metz et al. 2004). We point out that adopting the distance of 13.8 Mpc ($m - M = 30.7$ mag) suggested by Saviane et al. (2004) would result in an overall shift of *all* absolute magnitudes by 0.7 mag towards fainter magnitudes, leaving the arguments presented in this paper unaltered.

Whitmore & Zhang 2002, Fall et al. 2005; for SCs in the extended tidal tails see Knierman et al. 2003) and the SC complexes (see e.g. Whitmore et al. 2005, Bastian et al. 2006) have been studied extensively. In addition, the Antennae galaxies are a testbed for a large number of studies related to star formation and dynamical evolution in such a complex environment (see e.g. Barnes 1988, Mirabel et al. 1998, Hibbard et al. 2001, Fabbiano et al. 2003, Metz et al. 2004, Wang et al. 2004, Hibbard et al. 2005).

The LF of the YSCs in the Antennae galaxies have been studied extensively. However, so far no consensus about the shape of the LF has been reached: see Fritze-v. Alvensleben (1999) in favour for a Gaussian shape, Whitmore et al. (1999) and Mengel et al. (2005) for a broken-power-law shape (this could be interpreted as intermediate case, with the shallower slope at the faint end equivalent to the Gaussian approaching the turnover, although Gieles et al. 2006 interpret this broken power-law as a sign of a physical upper mass limit of star clusters) and Whitmore & Schweizer (1995), Zhang & Fall (1999) in favour for a power law shape.

Establishing whether or not the LFs of SC systems are the same or different in quiescently star-forming galaxies compared to merger-induced starbursts has far-reaching implications for our understanding of the star formation and star cluster formation processes themselves and their presumed universality, and possibly of their environmental dependence. To assess whether or not there is a clear turnover in the SC LFs (Section 4), we introduce statistical methods to model the sample selection procedure (Section 4.1), which includes parametric modelling of the completeness function (our completeness studies for the Antennae's SC system are summarised in Section 2.2) and, in a second step, a maximum likelihood procedure to estimate the parameters of a power-law and a Gaussian distribution, respectively, from the data as modified by this completeness function. Applying a likelihood ratio test and Monte-Carlo simulations to test its significance we find statistically significant evidence for the presence of a Gaussian-like turnover[3] in the LF at absolute magnitudes between -9.5 and -8.0 mag in the U, B, and V bands, and at ≈ -6.5 mag in the I band (although less significant, at a 68 per cent level). These results are presented in detail in Section 4.2.

To investigate the robustness of these results, in Section 4.4 we study subsets of the full sample, divided according to various criteria. Although details change, the conclusions are confirmed by these tests. The implications of our results are discussed in Section 5.

2 OBSERVATIONS AND DATA REDUCTION

We reanalyse the most homogeneous dataset of broadband imaging observations of the Antennae system available to date, obtained using the *Hubble Space Telescope (HST)*/Wide Field and Planetary Camera-2 (WFPC2) as part of programme GO-5962 (PI B. Whitmore; see Table

Table 1. Observation log. All data obtained in Cycle 5 (in January 1996), using the *HST*/WFPC2 camera.

Filter	Johnson equiv. passband	total exposure time (s)
F336W	U	4500
F439W	B	4000
F555W	V	4400
F814W	I	2000

1). The images were retrieved via the on-the-fly data reduction pipeline OPUS from the *HST* data archive at the Space Telescope European Coordinating Facility (ST-ECF).

The image alignment and cosmic-ray rejection were done using standard tasks in IRAF, including tasks from STSDAS[4].

The source identification was done using a version of DAOPHOT, adapted to run under IDL. Since we do not *a priori* know whether or not the potentially young SCs we are seeking are dynamically relaxed, we relaxed the roundness and sharpness criteria slightly compared to the default values. We compared the number of objects found using flux thresholds of $3\sigma_{bg}$ and $4\sigma_{bg}$, where σ_{bg} represents the r.m.s. of the background flux, but found virtually no difference. We used the $> 4\sigma_{bg}$ sources, because we expected other completeness-limiting aspects of the data analysis to have more severe impacts (see 2.2). Subsequently, we considered only sources present in either all of the UBV, or in all of the BVI images. This procedure prevents excluding either severely extincted clusters (possibly lacking U-band imaging) or extremely young objects (possibly lacking I-band data).

In total, we identified 7817 sources with fluxes above the threshold value in either of our three adjacent passband sets. However, as already shown by Whitmore et al. (1999) the majority of these sources are contaminating bright stars in the Antennae galaxies themselves. This is also clear from the estimated youth of the starburst, with a strong component within the last few $\times 10^7$ yr, as is apparent from the presence of a large number of HII regions (e.g. Neff & Ulvestad 2000) and the observation of Hα emission (e.g. Whitmore et al. 1999, see their Fig. 4). The number of bright supergiant-type stars, Luminous Blue Variables, and bright O-type stars is difficult to estimate, but it is expected to be large, with a fair number reaching absolute V-band magnitudes of ≈ -9 mag, and a few rare, Eta Carinae-type objects reaching even $M_V \approx -10$ mag. However, the further cluster selection criteria we will apply remove the vast majority of these because of their properties, particularly the extendedness criterion.

[3] i.e. at a confidence higher than 99.5 per cent (in fact, *none* of the 1000 simulated datasets shows a superiority of the Gaussian over the power law as strong as in the real data)

[4] The Image Reduction and Analysis Facility (IRAF) is distributed by the (U.S.) National Optical Astronomy Observatories, which is operated by the Association of Universities for Research in Astronomy, Inc., under cooperative agreement with the (U.S.) National Science Foundation. STSDAS, the Space Telescope Science Data Analysis System, contains tasks complementary to the existing IRAF tasks.

2.1 Photometry and cluster sizes

The crowding of the sources, their large number, partially their spatial extent and the strong variations in the galactic background contribution render photometry of the clusters extremely difficult. While the large number of sources requires some automation in source photometry and cluster candidate selection, this is severely hampered by the other factors indicated above.

Therefore, we developed an automated "cookbook" to improve aperture photometry by taking the sizes of the sources into account. For a number of cluster light profiles and a wide range of intrinsic cluster sizes we determined the "observed" size (as broadened by the point-spread function [PSF] and the diffusion kernel of the camera; the fitted profile used was a Gaussian, for simplicity and stability reasons) as well as the size-dependent aperture corrections (ACs) required to account for all of the cluster light (for a full description see Anders et al. 2006; hereafter AC/sizes Paper). In the present paper we will apply the algorithms presented and extensively tested in the AC/sizes Paper to the Antennae data.

To each of the 7817 sources we fit a Gaussian light profile, as justified and validated in the AC/sizes Paper, and obtain aperture photometry using 3-pixel source apertures, and 5/8-pixel inner/outer radius sky annuli. These sizes were chosen as a good compromise between being small enough to avoid crowding and the potentially detrimental effects caused by the highly variable background, and large enough to average out the Poissonian noise from the source flux and aperture centring effects.

Since the majority of the clusters are younger than 25 Myr (see Whitmore et al. 1999 and Section 4.3), we do not expect them to have already developed tidally-truncated King profiles (King 1962). We therefore assume the average profile representing the YSCs in the LMC, namely an Elson et al. (1987) (EFF) profile, with a power-law slope of -3, corresponding to an EFF15 profile in the BAOLAB software environment[5]. If the measured sizes in the different passbands differed, the luminosity-weighted mean of the measurements was taken as representative size. Throughout this paper we will use the FWHM of the EFF15 model as measure for the "size" of the objects, unless otherwise stated.

Using the size information just obtained and the aperture photometry of the clusters, we apply the recipes developed in the AC/sizes Paper, including size-dependent ACs and background-oversubtraction corrections. The total brightnesses were corrected for Galactic extinction (Schlegel et al. 1998), converted from the STMAG system of the *HST* observations to the VEGAMAG system[6], and subsequently transformed to absolute magnitudes.

For a source to be included in our final cluster sample it has to fulfil the following criteria:

- It must have been found by the DAOPHOT-like IDL routine.
- It must be detected at least in either all UBV or all BVI images, to filter out spurious detections and residual cosmic rays. In addition, since we want to determine physical parameters for these clusters using the ANALYSED algorithm (Anders et al. 004a) in a subsequent paper (Paper II), we need multi-passband photometry, ideally for a large number of passbands and a wide wavelength range.
- The size determination must have converged. We need to correct our photometry using the size-dependent ACs derived in the AC/sizes Paper. Therefore, size information is essential. However, the size determination becomes increasingly difficult and unreliable for faint objects, hence also reducing the sample's completeness (see Section 2.2).
- The converted (= *intrinsic*) FWHM must be in the range from 0.5 to 10 WF3 pixels (i.e., pixels on the wide-field-3 chip of the WFPC2 camera), corresponding to a FWHM of 4.6 to 93 pc (or a half-light radius $R_{1/2}$ of 5.2 to 105.1 pc, assuming an average young LMC "EFF15"-type cluster profile) at the adopted distance of the Antennae. This range covers the range for which the formulae derived in the AC/sizes Paper can be applied confidently. For clusters smaller than 0.5 WF3 pixel the correction equations determined in the AC/sizes Paper become inaccurate. In addition, the lower size cut-off at 0.5 pixel (imposed to ensure that the source is extended, and hence a likely cluster) significantly reduces the sample contamination by bright supergiants, which would appear as point-like objects: the observed size would be on the order of the filter-dependent PSF size ($\sim 1.5 - 2$ pixels). The upper size limit was chosen as a compromise in view of the contamination by cluster complexes and the number of sources. To satisfy both constraints we will, where appropriate, distinguish between SC samples characterised by sizes in the range from $R_{1/2} \simeq 5$ to 25 pc ("small" clusters) and our full sample. Note that cluster complexes in M51 and the Antennae have diameters of $\gtrsim 100$ pc (see Bastian et al. 005b, 2006).
- The photometric error in each passband must be $\leqslant 0.2$ mag, because we need accurate cluster photometry to determine the physical cluster properties within reasonable uncertainty ranges in Paper II.

The final full sample contains 752 clusters satisfying all of these constraints, the small cluster sample contains 365 clusters.

2.2 Completeness determination

In particular for a situation as complex as in the Antennae system, completeness determinations are as difficult as cluster selection and photometry.

The ultimate goal for the determination of the completeness function of a cluster sample is the determination of a local completeness fraction for each cluster, by taking into account all effects of the local environment of each cluster and all relevant selection effects.

In reality, at least the detailed spatial dependence of the completeness functions can hardly ever be determined accurately for each cluster. Here, we determine the completeness functions for two different cluster sizes (for intrinsic sizes of 1 and 2 pixels, chosen, respectively, to represent the size bin

---

[5] BAOLAB is a powerful image analysis suite, described in Larsen (1999). It is especially powerful for cluster size measurements of marginally resolved objects, and for the creation of artificial cluster images, and thus for detailed completeness tests.

[6] The additive offsets required are solely filter-dependent, as they result only from the different calibration spectra. They can be retrieved from the authors.
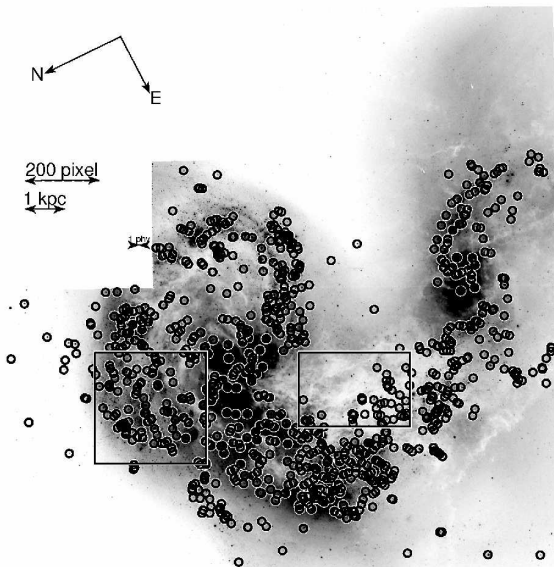
Figure 1. The Antennae galaxies, with the two regions for which the completeness functions were determined indicated: on the left-hand side the DISC region, on the right-hand side the OVERLAP region. The clusters are circled. Orientation and length scales indicated in the image.

with the largest number of clusters, and roughly approximating the median cluster size) in two distinct regions of the galaxies, distinguished by their average source density. The location of the regions are shown in Fig. 1. We labelled the regions DISC region (on the left-hand side, in the disc of NGC 4038) and OVERLAP region (on the right-hand side, in the region where the discs are overlapping, and the presence of large amounts of dust is seen in white).

For both regions, we performed a number of tests to estimate the completeness functions. For the DISC region we will present the different methods and compare their results (see Figs. 2 and 3). For the most sophisticated method (taking into account filter cross-correlation, photometric accuracy and the requirement for the cluster size determination to converge) we will show the results for the OVERLAP region as well (see Fig. 3). The results are summarised in Table 2.

The simplest way to estimate completeness functions is by distributing Gaussian-shaped artificial sources ("stars") with a range of brightnesses onto the image, e.g. by using the IRAF routine MKOBJ with radii corresponding to the PSF sizes, and then to determine the fraction of sources being recovered by the source finding algorithm. This can be done for each passband separately (see Fig. 2, upper panel, thin solid lines with symbols). However, for source identification we require that a detection must be positive in at least 3 adjacent passbands out of the 4 available. For this cross-correlation, a spectral energy distribution (SED) must be assumed. We investigated the cases of a flat SED (all colours are equal to 0, by definition), an SED representative of a young solar-metallicity cluster (age = 12 Myr, $Z = 0.02 = Z_\odot$), and one for an intermediate-age subsolar-metallicity cluster (age = 100 Myr, $Z = 0.008 = 0.4\ Z_\odot$); see the thin long-dashed lines in the upper panel of Fig. 2 for the results.

In addition, we require the clusters to have good pho-
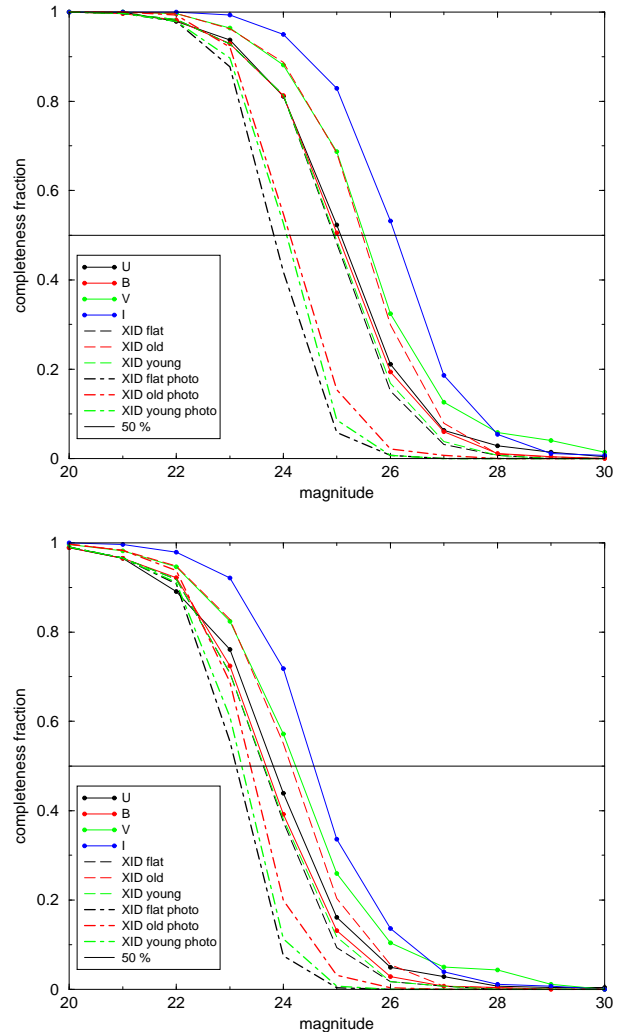

Figure 2. Upper panel: Completeness fractions based on artificial *stars*. Bottom panel: Completeness fractions based on artificial *clusters* with FWHM = 1 pixel. Thin solid lines with bullet points: Completeness functions for the individual filters. The horizontal axis is the magnitude in the respective passband. Thin dashed lines: Completeness functions for cross-correlating the filters. The horizontal axis is the magnitude in the V band. Thick dot-dashed lines: Completeness functions for cross-correlating the filters and requiring good photometry (uncertainties $\leqslant 0.2$ mag). The horizontal axis is the magnitude in the V band. XID = cross-correlation. Both panels relate to the DISC region.

tometry, with photometric errors smaller than 0.2 mag in each passband. This requirement further decreases the completeness fractions. The results are shown in the upper panel of Fig. 2 by the thick dot-dashed lines.

However, neither the Gaussian shape nor the small size of the artificial stars are realistic representations of a YSC. We therefore built more realistic cluster models (with intrinsic FWHM = 1 and 2 pixels, as explained above), using BAOLAB, taking both the appropriate HST/WFPC2 PSFs (based on the TINY TIM software package; see Krist & Hook 2004) and the HST/WFPC2 diffusion kernel into account. We then performed the detection, cross-correlation and pho-
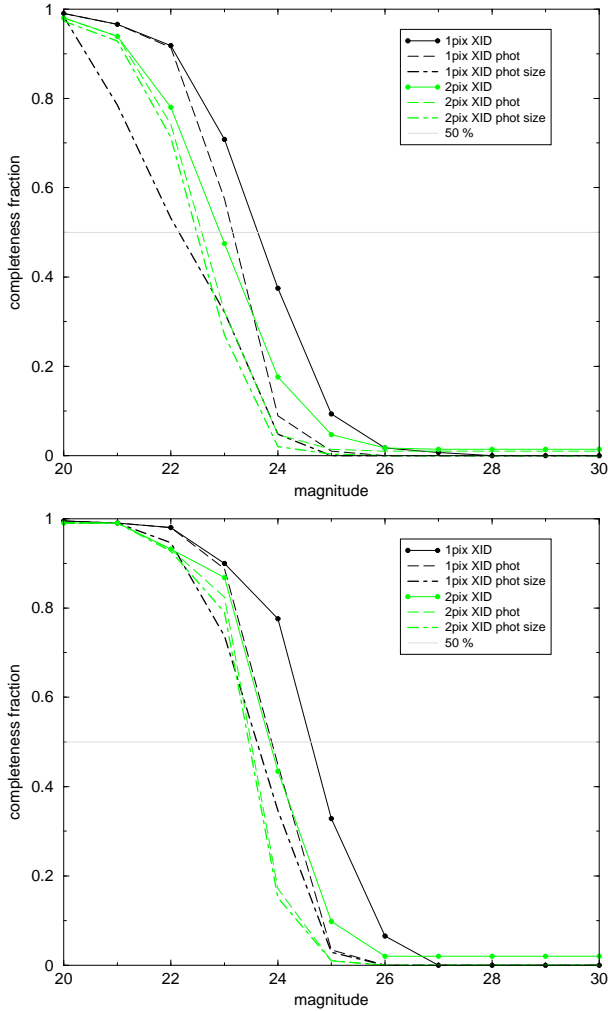
Figure 3. Completeness fractions based on artificial clusters, taking the cluster sizes and size determination effects into account. Black lines correspond to clusters with intrinsic FWHM = 1 pixel, light grey lines (in colour print: green lines) to clusters with intrinsic FWHM = 2 pixels. Solid thin lines with bullet points: only cross-correlation (here only the cross-correlations using the flat SED are shown, for reasons of clarity). Long-dashed thin lines: cross-correlation including photometric accuracy determination; thick dot-dashed lines: full completeness fractions including size determination. Upper panel: DISC region, bottom panel: OVERLAP region. XID = cross-correlation.

tometry tests once again. The results are shown in the bottom panel of Fig. 2.

For the real clusters an additional constraint imposed is the size determination. Hence for each cluster the size determination has to converge. Since the size fitting will not converge easily for faint clusters, this further reduces the completeness fraction of the source detections. In addition, all methods are sensitive to the cluster size. These results are given in Fig. 3, which also provides the comparison between the completeness determined in the DISC region with that for the OVERLAP region.

Table 2. Comparison of 50 per cent completeness limits for artificial sources of different types (stars versus clusters; 2 cluster sizes), different regions within the Antennae system, and different methods of completeness determination. XID = cross-correlation.

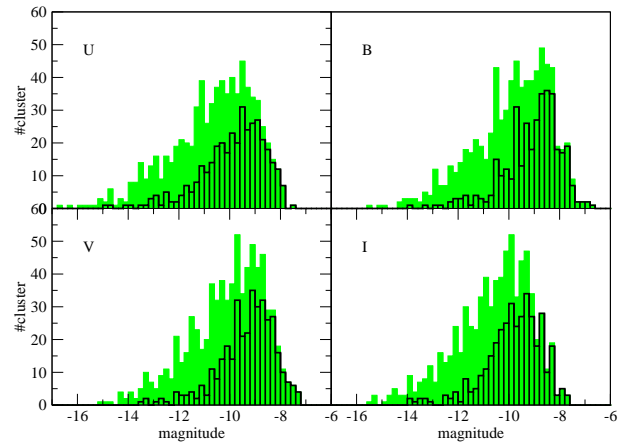| model	star DISC	cluster DISC 1 pix	cluster DISC 2 pix	cluster OVERLAP 1 pix	cluster OVERLAP 2 pix
50 per cent completeness limits in individual passbands					
U only	25.1	23.8	23.2	24.6	24.0
B only	25.0	23.7	23.1	24.8	24.1
V only	25.5	24.2	23.6	25.3	24.5
I only	26.1	24.6	24.1	25.2	24.6
50 per cent completeness limits of cross-correlated data					
XID only	24.9	23.6	22.9	24.6	23.8
phot	23.8	23.2	22.6	23.9	23.5
phot + size	–	22.2	22.5	23.6	23.5

Figure 4. LFs of the final cluster sample in the four passbands, not corrected for the effects of sample (in)completeness. The shaded histogram shows the full cluster sample, the open histogram represents the small cluster sample.

3 LUMINOSITY FUNCTIONS

Fig. 4 shows the cluster LFs, i.e. the number of clusters per magnitude bin, for the four passbands. While the LFs appear to exhibit a turnover, the decrease at the faint end is (at least partially) caused by the observational incompleteness. To separate the effects of (in)completeness from a possible intrinsic decrease in the number of faint clusters (i.e. an intrinsic turnover), we designed the statistical tools described in Section 4.

3.1 Comparison with data in the literature

The pioneering work of Whitmore and collaborators has resulted in the largest homogeneous dataset of star cluster photometry for the Antennae system. For a direct comparison Brad Whitmore kindly provided us with the photometry of their full (unpublished) source sample.

Comparison of luminosity functions for Antennae sources

Our data: black open + blue dashed fit; Whitmore et al 99: green filled + dark green solid fit
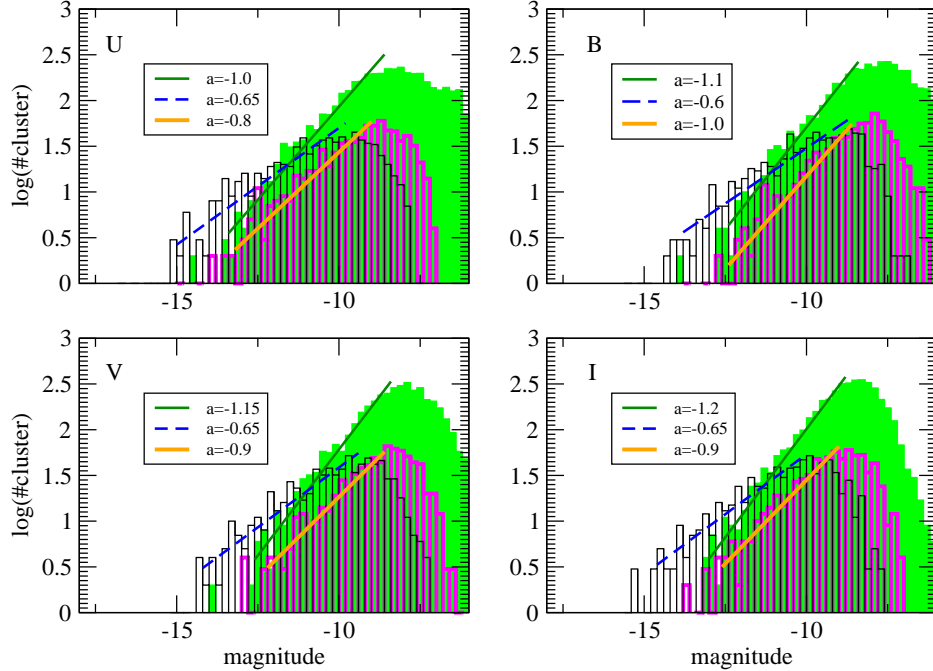Our data without ACs: magenta open + orange fit

Figure 5. LFs of the final cluster sample in the four passbands, compared to the corresponding data from Whitmore et al. (1999). The slopes, a, of the linear fits to the logarithms of the LFs are indicated in the legends. This slope is equivalent to the LF power-law slope α_{LF}.

As can be seen from Fig. 5, our LFs are substantially flatter than those of the Whitmore sample. This can be partially attributed to the effect of the ACs: bright clusters in our sample tend to be larger (i.e. have larger ACs), which flattens the LF. Overall, our sample without the ACs is in better agreement with the Whitmore sample (despite the vastly different sample sizes). In addition, the different selection criteria probably also play an important role in the slope differences, as our selection criteria largely exclude the stellar contamination discussed in Whitmore et al. (1999), which is expected to dominate the faint end of the LF and thus will lead to a steepening of the LF.

4   TURNOVER DETERMINATION

Particularly important for our study of the LFs is the potential existence and the location of a turnover in our dataset to establish the link between our YSCs and the old GCs. Unfortunately, the completeness function drops off already at significantly brighter magnitudes. This results in an apparent turnover of the *observed* cluster luminosity distribution for any reasonable *intrinsic* luminosity distribution (which we call the ILF), like a power-law or Gaussian distribution. Therefore, the process that leads to the observations, has to be modelled carefully before any conclusion can be drawn with respect to the existence of a possible turnover.

In Section 4.1 we present a detailed statistical model for the observations and develop an appropriate statistical

procedure to test for the presence of a turnover. In section 4.2 we apply these methods to the Antennae YSC data.

4.1   Modelling the observations

The observed luminosity distribution is different from the "true" ILF by virtue of two different stochastic mechanisms. First, the observations are affected by measurement errors. Even more important though is a so-called "missing data" mechanism described, in essence, by the completeness function. Here, the probability of a cluster to be included in the observations X_i ($i = 1, \ldots, N$) depends on its brightness. The fainter the cluster, the less probable it is to be observed. Moreover, if the cluster is fainter than $M_V \approx -5$ to -6 mag, the completeness function approaches zero, and it is not possible to analyse this part of the LF at all. For a general introduction to statistical methods with missing data see, e.g., Little & Rubin (2002), for a biometric example see Patil & Rao (1978).

We now introduce the statistical model in more detail. Call f_ϑ the (*intrinsic*) LF, i.e. the (probability) density of the brightness of a cluster, and assume that the intrinsic luminosities of the Antennae clusters are realisations, m_i, of independent random variables, M_i, distributed according to f_ϑ. Here, upper-case letters indicate random variables, and lower-case letters their realisations (i.e. the observed value). In the literature, essentially only log-normal ("Gaussian") and power-law models are under consideration for f_ϑ, where

ϑ are the parameters of the model, to describe the LFs of star clusters.

Please note: We are going to fit both the Gaussian and the power-law models to the distribution of cluster magnitudes. Although in the literature the power-law models are generally fitted to the luminosity distributions, our method is a conservative approach, as it assigns less weight to the (potentially less well-defined) faint end. Hence, if we can show that a power law model for the cluster magnitudes predicts too many faint clusters, this would, a fortiori, hold for a power law in cluster luminosities.

Even if the completeness function would be unity for all magnitudes, the measurements would not be equal to the m_i, but scatter around these true values due to measurement errors. We call $e(\cdot|M)$ the probability density of the measurement error of a cluster with intrinsic brightness M. More formally, $e(\cdot|M)$ is the *conditional density* of the measurement errors given that the intrinsic cluster brightness is M, i.e. the probability density that the measurement error has a certain value if we already know that the intrinsic brightness is M. Then, the *observable* brightness is given by the random variable $Y_i = M_i + E_i$, where the E_i are distributed independently of each other, as $e(\cdot|M_i)$. We call Y_i the *observable* brightness, as opposed to the *observations* X_i, since not all of the clusters (with *observable* brightness Y_i) will actually be included in an observed sample due to the (in)completeness effects.

The error density $e(\cdot|M)$ can, for example, be a Gaussian density with fixed variance, i.e. independent of M, or a Gaussian with a variance which depends on M. Since the observed values basically result from photon count data, a Poisson distribution with expected value computed from M_i is another straightforward possibility. We use the latter choice. However, computations where we assumed Gaussian noise yield very similar results. This is because the measurement errors are small, and in particular modify the observed cluster distribution much less than the missing data effect described next.

The probability of a cluster with observable brightness Y to be included in the observations is given by the completeness function $c(Y)$. We model this by a random variable Z which is Bernoulli distributed with parameter $c(Y)$, i.e. Z is 1 with probability $c(Y)$, and 0 otherwise.

Recapitulating, the observable brightness is modelled as pairs (Y_i, Z_i), $i = 1, \ldots, N$ of a random variable $Y = M + E$ with probability densities f_ϑ of M, $e(\cdot|M)$ of E, and g_ϑ of Y, and a second random variable Z, which is Bernoulli distributed with parameter $c(Y)$. The observations consist of those pairs (Y_i, Z_i) where $Z_i = 1$. This implies that the probability density h of an observation X_i is the joint density p_ϑ of the pair (Y, Z) conditioned on the event $Z = 1$:

$$h(x) = p_\vartheta(x|z = 1) = \frac{p_\vartheta(x, z = 1)}{P_\vartheta(Z = 1)},$$

where $P_\vartheta(Z = 1)$ is the (marginal) probability that $Z = 1$.

In the remainder of this section we describe our estimator for the best-fit values $\hat{\vartheta}^{\mathrm{mod}}$ of the parameter(s) ϑ for the Gaussian and power-law models, respectively, i.e. "mod" reads either as "Gaussian" or "power law". Our approach is based on maximum likelihood estimation, which amounts to maximising the probability of the observed data

$(Y_i, Z_i = 1)$, $i = 1, \ldots, n$, given the model "model" with parameter(s) ϑ, i.e.

$$\hat{\vartheta}^{\mathrm{mod}} = \mathrm{argmax}_\vartheta \mathcal{L}_\vartheta(X_1, \ldots, X_N),$$

where

$$\mathcal{L}_\vartheta(X_1, \ldots, X_N) \equiv \prod_{i=1}^{n} p_\vartheta^{\mathrm{mod}}(X_i|z = 1),$$

and $p_\vartheta^{\mathrm{mod}}(Y = X_i|z = 1)$ is the (conditional) probability of a cluster to have observable brightness X_i given $Z = 1$, i.e. to be actually contained in the observations. To compute this conditional density we first determine the marginal probability that $Z = 1$ as

$$P_\vartheta^{\mathrm{mod}}(Z = 1) = \int_{-\infty}^{\infty} p_\vartheta^{\mathrm{mod}}(z = 1|y)g_\vartheta^{\mathrm{mod}}(y)\mathrm{d}y$$

$$= \int_{-\infty}^{\infty} c(y) \left[\int_{-\infty}^{\infty} p_\vartheta^{\mathrm{mod}}(y|m)f_\vartheta(m)\mathrm{d}m \right] \mathrm{d}y.$$

Here we use that $p_\vartheta^{\mathrm{mod}}(z = 1|Y) = c(Y)$ (i.e. does not depend on the specific model at all) and

$$g_\vartheta^{\mathrm{mod}}(y) = \int_{-\infty}^{\infty} e(y - m|m)f_\vartheta^{\mathrm{mod}}(m)\mathrm{d}m.$$

Here, $e(y-m|m)$ is the probability that $Y = y$ given $M = m$. Moreover,

$$p_\vartheta^{\mathrm{mod}}(x, z = 1) = p_\vartheta^{\mathrm{mod}}(z = 1|x)g_\vartheta^{\mathrm{mod}}(x)$$

$$= c(x) \int_{-\infty}^{\infty} e(x - m|m)f_\vartheta^{\mathrm{mod}}(m)\mathrm{d}m.$$

Therefore, the likelihood function of the observations $X_1, \ldots, X_N$ is

$$\mathcal{L}_\vartheta^{\mathrm{mod}}(x_1, \ldots, x_N) = \prod_{i=1}^{n} \frac{c(x_i) \int_{-\infty}^{\infty} e(x_i - m|m)f_\vartheta^{\mathrm{mod}}(m)\mathrm{d}m}{P_\vartheta^{\mathrm{mod}}(Z = 1)^n}.$$

Maximisation of $\mathcal{L}_\vartheta^{\mathrm{mod}}(X_1, \ldots, X_N)$ yields the estimators ("best-fit parameter(s)") $\hat{\vartheta}^{\mathrm{mod}}$. Moreover, we assign the likelihood to the respective model under consideration as a measure of its "probability" given the data. This can be used to select the best model, particularly by comparing the ratio of the likelihoods of the best-fit Gaussian and power-law model in a likelihood ratio test. Versions of this kind of model selection are well established for a broad range of statistical applications (see e.g. Lehmann 1994).

4.2 Statistical significance of a turnover in the ILF

We now discuss the results of our application of this method to the Antennae clusters. For simplicity, we parametrise the completeness functions as Fermi functions,

$$(1 + \exp(a(x - b)))^{-1} \qquad a, b \in \mathbb{R}.$$

We emphasise that the general results do not change if we use, e.g., interpolation methods to describe the completeness function.

For the V band, the completeness data as determined in Section 2.2 (crosses) and the fitted parametrisation (solid line) are shown in Fig. 6. Three completeness fractions were determined per magnitude, corresponding to the three different cluster SEDs considered, giving some uncertainty estimate. The fit was performed as L_1 – Fit (i.e. by minimising the absolute distance between model function and simulated completeness fractions).

Fig. 7 shows the best fits for the Gaussian and the power-law models for the different passbands. A visual inspection of Fig. 7 already indicates that the intrinsic Gaussian models fit better, particularly with respect to the faint tail of the LF. The intrinsic power-law models fit quite well in all bands for bright magnitudes but assign too much weight (i.e. predict too many clusters) to the faint magnitudes. One might suspect that this is due to the completeness curve assigning too much probability to that magnitude range. However, an inspection of Fig. 6 shows that for $-7 \leqslant M_V \leqslant -6$ mag, where the power law predicts too many clusters, the completeness curves estimate the generated completeness fractions without significant bias. This observation can also be made for the other bands. Moreover, fitting a different completeness curve (e.g., a linear interpolation of the mean/median of the completeness fractions at each magnitude) leads to the same effects. One has to keep in mind that the completeness fraction plays a crucial role when fitting a model in this context.

More robust conclusions can be drawn using the model likelihoods. To test the (null) hypothesis "true model is power law with the estimated best fit parameters" against the alternative of a Gaussian density we use a Likelihood Ratio test (cf. Lehmann 1994). We first simulate the distribution of the ratio of the likelihoods of a Gaussian and a power-law model under the hypothesis that the power-law model holds true. This means that we randomly draw a number of observations equal to the number of data point from the fitted power-law model (using the fitted completeness curves) and then again fit a power law and a Gaussian model and calculate the ratio of the corresponding likelihoods. This procedure is repeated 1000 times and the empirical quantiles of the resulting distribution are compared to the observed likelihood ratio of the data. Table 3 shows that the probability to erroneously reject the null hypothesis is at a level of less than 0.5 per cent for the U, B and V band, i.e. the result is "strongly significant" (in fact, for most cases considered *none* out of 1000 simulations, where the ILF is *assumed* be a power-law, shows a superiority of the Gaussian over the power-law as strong as in the real data). Note, that we *estimate* the probability of erroneously rejecting the null hypothesis from the rate of rejecting the power law in favour of a Gaussian in simulations with artificial data generated from the power law model. Here, the result of zero rejects out of 1000 simulations implies an *estimate* of the *true rate of rejection* in the simulations of $p \leqslant 0.5\%$, with an error probability of this claim to be wrong of $\lesssim 1\%$, based on the characteristics of Bernoulli-distributed random variables. For the I band, the observed value is greater than 74 per cent of the simulated values. This means that the corresponding probability of erroneous rejection (i.e. the corre-

Table 3. Results of the Likelihood Ratio tests. For clarity the difference of the negative log-likelihood values is given instead of the likelihood ratios. Hence, negative values indicate that the null hypothesis (i.e. power law) is superior. The last column gives the probability of error for discarding an intrinsic power law (hence small values represent the inferiority of the power law).

Filter	50%	Quantiles 95%	99%	100%	**Obs.**	Prob.
U	-4.5	0.1	2.5	5.0	**15.5**	0.000
B	-6.0	-0.9	1.3	6.2	**32.5**	0.000
V	-5.4	-0.05	2.5	9.4	**15.3**	0.000
I	-1.2	1.8	3.2	5.5	**-0.4**	0.322
FWHM=0.5-2.36 pixel → $r_{1/2} \simeq$ 5-25 pc						
U	-0.9	2.6	5.0	6.8	**18.5**	0.000
B	-1.3	3.0	4.6	8.9	**35.5**	0.000
V	-0.5	4.0	5.9	8.9	**30.8**	0.000
I	-0.1	3.4	5.2	7.7	**16.8**	0.000

Table 4. Best-fitting parameters for the Gaussian model. (μ = mean)

Filter	Gaussian μ	95 percentile range μ	σ
U	-9.0	[-9.4:-8.5]	2.3
B	-8.8	[-9.0:-8.5]	2.0
V	-8.5	[-8.8:-8.1]	2.1
I	-6.2	[-7.3:-5.0]	2.7
FWHM=0.5-2.36 pixel → $r_{1/2} \simeq$ 5-25 pc			
U	-8.6	[-8.9:-8.2]	1.7
B	-8.3	[-8.5:-8.0]	1.4
V	-8.4	[-8.6:-8.1]	1.4
I	-8.0	[-8.4:-7.5]	1.5

sponding p-value) is 0.322 (i.e. 32.2 per cent) and the null hypothesis cannot be rejected at any reasonable level.

In Table 4 we present the parameters and the uncertainty ranges from bootstrapping for the best-fitting Gaussian models.

We conclude that the statistical methods yield important evidence against power-law-like distributions for our dataset, thus hinting at the presence of a turnover in the ILF at absolute magnitudes between -8.0 and -9.5 mag in the $U, B,$ and V band. In the I band, the different models seem to fit the data with the same quality. Note that even an ILF that is flat to the right of the peak of its best-fit Gaussian would predict too many faint clusters, because even a Gaussian distribution predicts rather too many than too few faint clusters. However, such a model is at the borderline between any possible presence and absence of a turnover in the intrinsic distribution. In particular, a rising ILF such as a power law is even less likely.

4.3 Cluster ages, cluster masses and infant mortality

We determined ages from our broad-band photometry using the AnalySED algorithm, described in Anders et al.
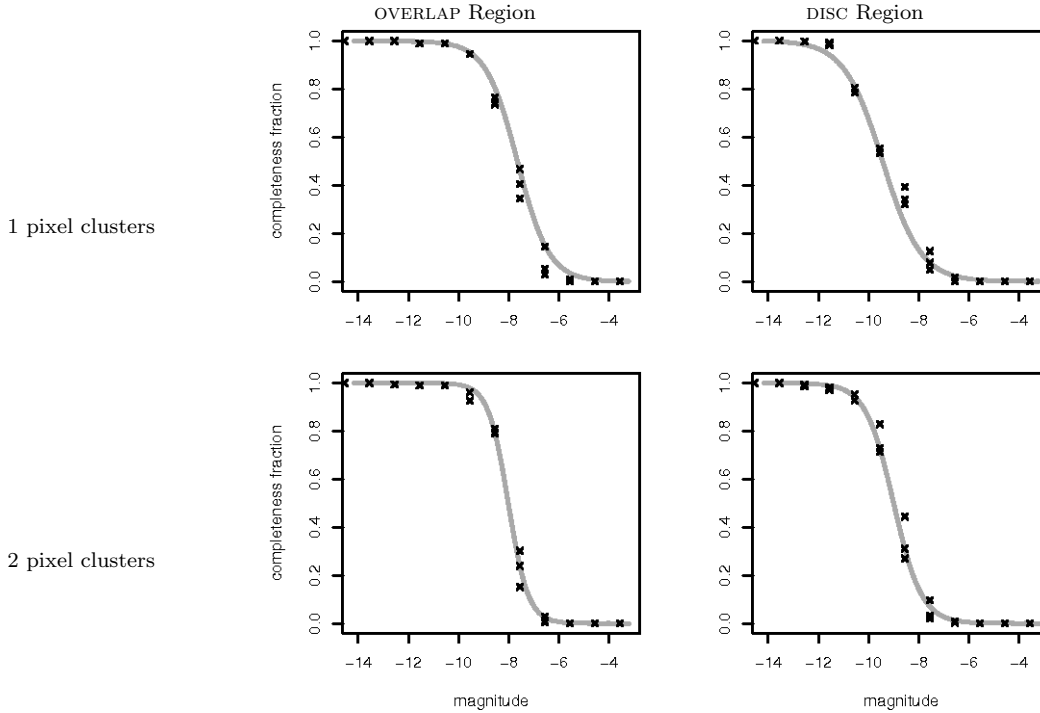
Figure 6. The completeness curve fits determined for the *V* band. Crosses: Data points from completeness tests. Gray solid line: Fermi function fit to the data points. Note that for different bands only the location on the magnitude axis varies but not the shape of the curve.

(004a). Both the best ages and representative 1σ uncertainty ranges are shown in Fig. 8. Combining the average age of our full cluster sample of ≈ 25 Myr and solar metallicity with the parameters in Table 4 yields the following parameter estimates for the MF: $\log(M_{\rm TO}[{\rm M_\odot}]) = 4.2$ and $\sigma_M = 0.85$ dex. Compared to the values for the Milky Way (see e.g. Ashman & Zepf 1998, $\log(M_{\rm median}[{\rm M_\odot}]) = 4.9$, $\log(M_{\rm mean}[{\rm M_\odot}]) = 5.3$, $\sigma_M = 0.49$ dex), this turn-over appears to be shifted to lower masses, and to be broader. Note that we prefer to apply our statistical treatment to the luminosities rather than to the (physically more relevant) cluster masses, because the crucial completeness determination can be performed accurately only for the (observed) magnitudes and not for the (derived) masses.

Observations of increasing numbers of interacting and starburst galaxies show a significantly larger number of young ($\lesssim 10-30$ Myr) star clusters than expected from a simple extrapolation of the cluster numbers at older ages, under the assumption of a roughly constant star cluster formation rate over the host galaxy's history, and taking into account the observational completeness limits as well as the effects of sample binning (see de Grijs & Parmentier 2007 for an in-depth review). The current consensus is that an initial fast ($\lesssim 10-30$ Myr) disruption mechanism can effectively remove up to 90 per cent of the youngest, short-lived clusters from a given cluster population. This process has been coined cluster "infant mortality" (Whitmore 2004).

Taking the best ages in Fig. 8 at face value, the time-scale of infant mortality appears to be around 18-25 Myr (depending on the binning in age), in rough agreement with previous claims (see e.g. Whitmore 2004, Fall et al. 2005, Mengel et al. 2005; see also Whitmore et al. 2006 for a presentation of earlier results), but perhaps somewhat shorter
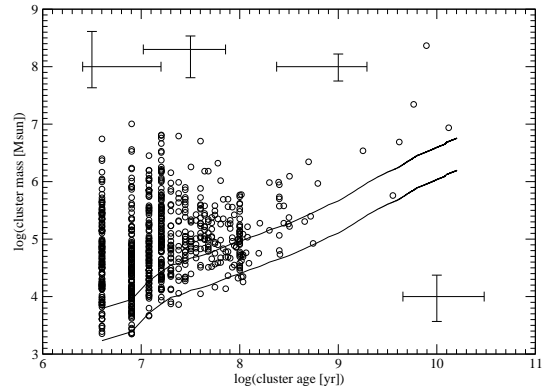

Figure 8. Age-vs.-mass relation for the full cluster sample. In the lower-right corner mean error bars for all clusters are shown. The upper error crosses give the mean uncertainties for clusters with ages < 10 Myr, between 10 and 100 Myr and > 100 Myr, respectively. The solid lines represent the fading lines, as given by the GALEV models (solar metallicity, see Anders & Fritze-v. Alvensleben 2003) and the completeness limits determined in Section 2.2. Both lines correspond to the completeness curves for artificial clusters with 1 pixel size. Upper line: DISC region. Lower line: OVERLAP region.

than theoretical predictions by Goodwin & Bastian (2006), possibly due to the high galactic background and/or the violent environment. Assuming a constant cluster formation rate during the last $\lesssim 100$ Myr the infant mortality rate is of order 60 per cent, i.e. ≈ 40 per cent of the newly formed clusters survive the first ≈ 25 Myr.
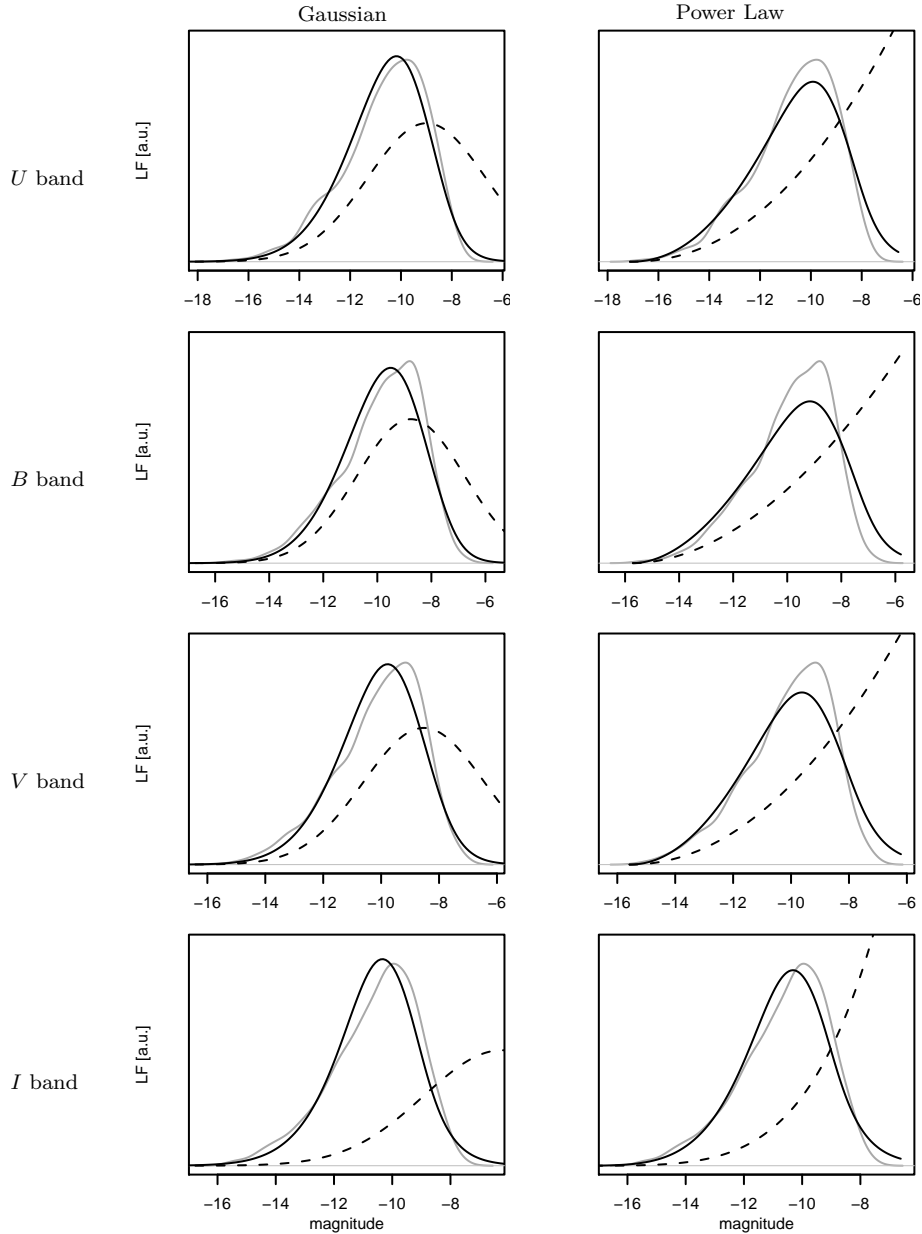
Figure 7. Fits of the Gaussian and the power-law model for the different passbands. The grey line is a kernel density estimate of the observed data and the black line shows the Maximum Likelihood fit multiplied by the weighted sum of the completeness curves (with weights chosen according to the relative frequencies of observations for the different regions and cluster sizes). The dashed line corresponds to the estimated LF without considering the completeness. The vertical scaling is in arbitrary units (a.u.), but scaled such that the modelled LF (i.e., the ILF convolved with the distribution of observational errors, multiplied with the completeness function) gives the same number of clusters as observed.

4.4 Investigating subsets of the full cluster sample

In this section we investigate the existence of a turnover in the LFs of subsets of the full cluster sample, using our newly developed statistics tools (Section 4.1). We limit these analyses to the V-band magnitudes.

First, we analysed the photometric data not corrected for size-dependent ACs, in order to exclude the possibility of calibration errors from the sizes/AC algorithm. The data for the V band are shown in Table 5.

In addition, we study three subsamples in cluster size (radius) and several subsamples in cluster age.

Two of the three size bins were chosen to be centred around the cluster sizes we studied the completeness functions for previously. The third bin contains all clusters larger than in the first two bins.

First, we chose three age bins roughly equally spaced in log(age/yr). In addition, we investigated subsamples which are (or are not) expected to be affected by infant mortality: following the theoretical work by Goodwin & Bastian (2006) we divided the cluster sample in clusters younger and older than 50 Myr. As a second test, based on the observed age distribution of our Antennae cluster sample, we divided the cluster sample into clusters younger and older than 25 Myr,

Table 5. Results of the Likelihood Ratio tests for several subsets, performed for the V band. For clarity, the difference of the negative log-likelihood values is given instead of the likelihood ratios. Hence, negative values indicate that the null hypothesis (i.e. power law) is superior. The last column gives the probability of error for discarding an intrinsic power law (hence small values represent the inferiority of the power law). The *italic* values are for clusters in the size range FWHM=0.5-2.36 pixel $\rightarrow r_{1/2} \simeq$ 5-25 pc.

Subset	#	50%	Quantiles 99%	100%	**Obs.**	Prob.
Without ACs						
V band	752	-0.8	4.9	7.6	**20.2**	0.000
V band	*365*	*-0.2*	*5.7*	*11.4*	***23.1***	*0.000*
Radius bins						
< 1.5 pix	275	-0.2	6.2	8.0	**27.5**	0.000
[1.5:2.5] pix	104	-0.6	2.0	3.7	**2.6**	0.004
> 2.5 pix	373	-8.0	-0.4	1.1	**24.4**	0.000
Age bins						
$\leqslant$ 12 Myr	382	-3.9	2.4	9.4	**4.8**	0.001
[16:100] Myr	328	-2.2	3.0	6.9	**8.7**	0.000
> 100 Myr	42	-0.6	2.2	3.5	**0.4**	0.118
< 25 Myr	541	-5.4	1.9	5.7	**5.0**	0.001
> 25 Myr	211	-0.8	4.2	7.5	**13.5**	0.000
< 50 Myr	627	-5.7	2.0	7.5	**10.6**	0.000
> 50 Myr	125	-0.4	3.8	6.6	**7.2**	0.000
$\leqslant$ 12 Myr	*179*	*-0.6*	*4.2*	*6.8*	***9.1***	*0.000*
[16:100] Myr	*163*	*-0.4*	*4.3*	*6.2*	***20.4***	*0.000*
> 100 Myr	*23*	*-1.6*	*1.8*	*3.4*	***0.8***	*0.054*
< 25 Myr	*254*	*-0.9*	*4.5*	*7.7*	***14.3***	*0.000*
> 25 Myr	*111*	*0.5*	*5.0*	*6.5*	***20.1***	*0.000*
< 50 Myr	*291*	*-0.8*	*4.8*	*6.6*	***19.8***	*0.000*
> 50 Myr	*74*	*-2.7*	*3.4*	*8.2*	***6.5***	*0.002*

as this seems to be the disruption time we see in our cluster sample.

As can be seen from Table 5, all but one of the subsets considered confirm the findings for the full data set. The only exception involves clusters with ages > 100 Myr, but these subsets consist of 23/42 clusters, too few to base unambiguous statistical conclusions on.

No significant difference is seen for the subsets during or after the infant mortality phase.

4.5 Investigating the effects of artificial decrease of completeness

We performed tests with the completeness functions artificially degraded, using offsets of 0.5 mag, 1 mag and 2 mag. The results are shown in Tables 6 and 7 and in Fig. 9.

As one might expect, the resulting best-fit model LFs become more and more skewed towards the bright end with increasing offsets, becoming increasingly unlike the observed distribution. For the full cluster sample, the power-law ILF becomes increasingly superior with increased offsets, as one might expect. For the sample containing only the "small" clusters, the superiority of the Gaussian is retained even

Table 6. Results of the Likelihood Ratio tests for either the full sample or the subset with half-light radii between $\simeq$ 5 and 25 pc, for different artificial shifts in the completeness functions, performed for the V band. For clarity, the difference of the negative log-likelihood values is given instead of the likelihood ratios. Hence, negative values indicate that the null hypothesis (i.e. power law) is superior. The last column gives the probability of error for discarding an intrinsic power law (hence small values represent the inferiority of the power law). These values relate to Fig. 9.

Subset	#	50%	Quantiles 99%	100%	**Obs.**	Prob.
Shift by 0.5 mag, all clusters						
V band	752	-1.9	4.0	5.8	**1.3**	0.072
Shift by 1.0 mag, all clusters						
V band	752	-1.1	3.0	6.1	**-3.3**	0.971
Shift by 2.0 mag, all clusters						
V band	752	-3.9	0.6	16.3	**-11.2**	1.000
Shift by 0.5 mag, small clusters						
V band	365	-0.1	5.3	7.0	**17.9**	0.000
Shift by 1.0 mag, small clusters						
V band	365	0.2	5.5	9.8	**15.6**	0.000
Shift by 2.0 mag, small clusters						
V band	365	1.0	6.3	8.6	**21.6**	0.000

by degrading the completeness. This follows naturally from intrinsic selection effects in which larger clusters of a given brightness will more easily be missed in our sample selection than smaller clusters, owing to their lower surface brightnesses.

For the full cluster sample the peak of the Gaussian distribution shifts strongly towards fainter magnitudes with increasing offset, i.e. in the range where the completeness functions are significantly greater than 0 both tested distributions resemble power laws. This effect is not as significant for the cluster sample with the narrower size range, again because of the intrinsic selection effects referred to in this respect.

5 DISCUSSION

5.1 Star Cluster Systems and their progenitors: LFs and MFs

The mass spectra of the SC progenitors, GMCs and GMC cores, in nearby galaxies are found to be of power law-type, with a slope of $-2.0 \lesssim \alpha \lesssim -1.5$ over a wide range of cloud and core masses (Solomon et al. 1987, Kramer et al. 1998, Zinchenko et al. 1998, Rosolowsky 2005, Rathborne et al. 2006), possibly with the exception of clouds in the outer parts of the Milky Way and in M33 (see Rosolowsky 2005), which might be represented by a steeper power law. All these galaxies, however, are neither currently interacting nor experiencing a strong starburst.
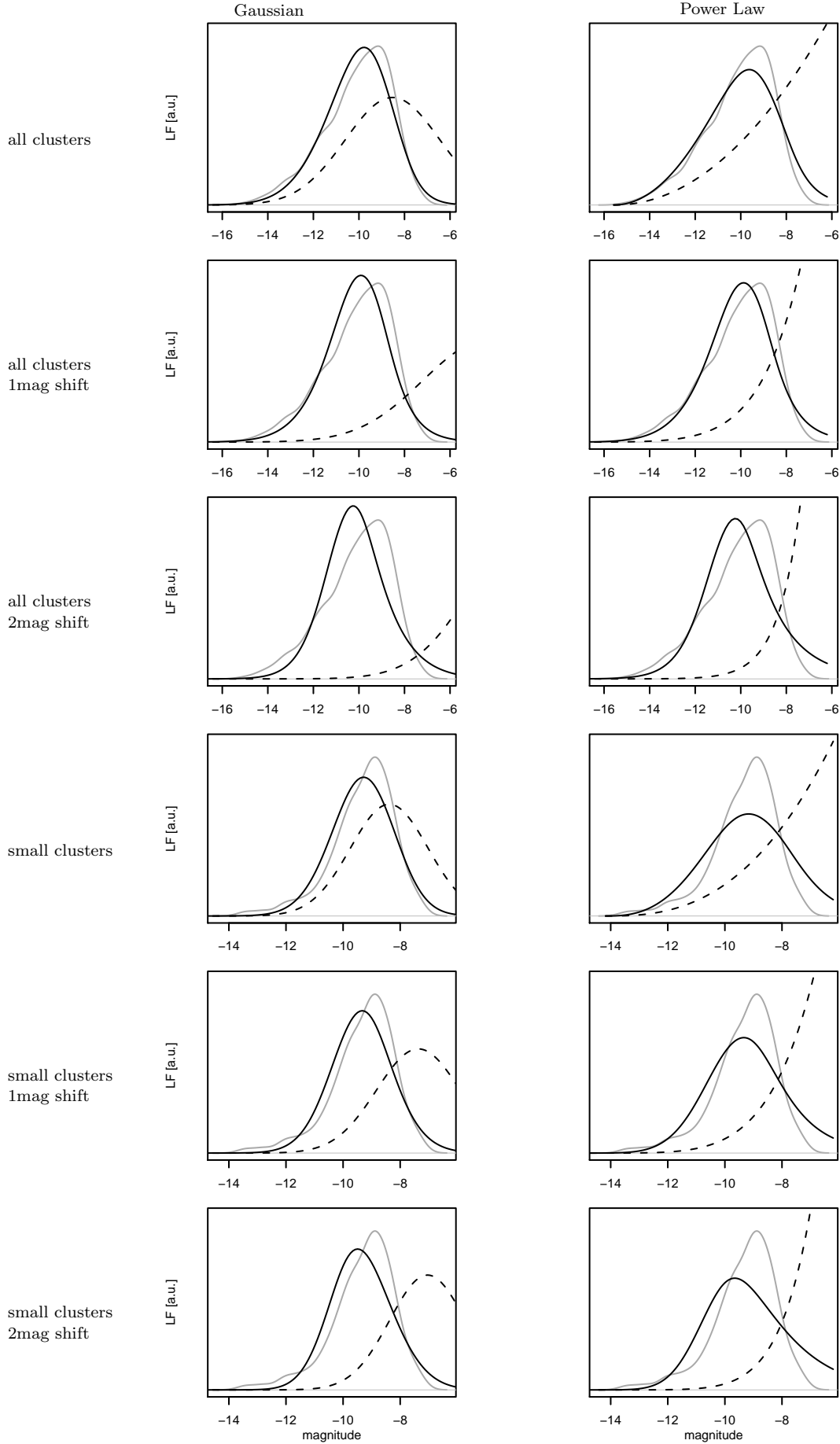
Figure 9. Fits of the Gaussian and the power-law model for the differently shifted completeness curves, V band only. The figure coding is as in Fig. 7.

Table 7. Best-fitting parameters for the Gaussian model, corresponding to Fig. 9 and Table 6.

Filter	μ	Gaussian 95 percentile range in μ	σ
Shift by 0.5 mag, all clusters			
V	-6.8	[-7.5:-5.9]	2.5
Shift by 1.0 mag, all clusters			
V	-4.4	[-5.6:-2.6]	2.8
Shift by 2.0 mag, all clusters			
V	-2.0	[-3.7:+0.7]	2.7
Shift by 0.5 mag, small clusters			
V	-7.8	[-8.1:-7.3]	1.5
Shift by 1.0 mag, small clusters			
V	-7.4	[-7.8:-6.8]	1.5
Shift by 2.0 mag, small clusters			
V	-7.0	[-7.5:-6.4]	1.3

A first attempt to assess the molecular cloud mass spectrum in the Antennae galaxies, by Wilson et al. (2003), revealed a power law with $\alpha \sim -1.4$ but remained limited to GMC masses above 5×10^6 M$_\odot$. Resolution of lower-mass molecular clouds, observations of molecular cloud cores and the determination of the cloud MF – *Is it different in massive gas-rich mergers compared to non-interacting galaxies?* – have to await commissioning of ALMA.

For old GC systems both LFs and MFs are of Gaussian shape: the LFs show a Gaussian turnover magnitude at $M_V = -7.3$ mag and a Gaussian $\sigma = 1.2$ mag. As GCs seem to be roughly coeval, at least within the associated uncertainties, with ages of 10–12 Gyr, the peaked luminosity distribution can be converted into a mass distribution. The corresponding peak mass occurs at $\sim 2 \times 10^5$ M$_\odot$. YSCs in the local Universe show LFs that appear generally characterised by power laws, at least towards the upper mass limit. It is not clear, however, whether or not the distinction between YSCs and GCs is meaningful for all galaxies, and whether it reflects an intrinsic difference in the nature of these clusters (i.e. their formation mechanisms) or originates from a initially universal continuous cluster distribution re-shaped by secular evolution and destruction of the lower-mass SCs.

Larsen (2004) reports the detection of so-called super star clusters (SSCs) in a number of seemingly undisturbed, quiescently star-forming face-on spirals. These SSCs are clearly very bright and very young; at least some of them have been shown to be very massive, too (Larsen et al. 2004). With masses around 2×10^5 to 1.5×10^6 M$_\odot$ and small radii (half-light radii between 3.0 and 5.2 pc; see Larsen et al. 2004), they resemble young GCs, although ongoing GC formation is not expected in these non-interacting, non-starbursting, just normally star-forming galaxies (see also Section 5.2). If these massive SSCs are not very rare exceptions, we would have to investigate where the descendants are of all those SSCs that presumably formed earlier

on, i.e. the intermediate-age GCs in those spirals, or whether we are witnessing a very special epoch in the star-formation history of those spirals.

Starburst and merging galaxies are observed to harbour rich systems of YSCs formed during the starburst event. Merger remnants with post-starburst signatures also reveal SC systems with ages of up to 1–3 Gyr (e.g., de Grijs et al. 003c, Goudfrooij et al. 2004), indicating that at least some fraction of these SCs formed during the burst survived much longer than most of the open clusters in the Milky Way.

The universality or non-universality (and possibly the environmental dependence) of the LFs of SC systems in quiescently star-forming galaxies compared to merger-induced starbursts provides important input for models of star and star cluster formation.

5.2 SC formation and star formation efficiencies

The lifetime of a SC depends on its mass (and stellar initial mass function), its initial degree of binding, and on its environment. While apparently all star formation is SC formation at the stage of embedded clusters in the Milky Way, most of the clusters are already unbound when they emerge from their dust cocoon (Lada & Lada 2003). Hydrodynamical cluster formation modelling has shown that very high SFEs are required to form a massive cluster that is long-term stable. The formation of a typical GC, sufficiently massive and strongly bound to survive for a Hubble time, requires a SFE of order 30 per cent or higher (Brown et al. 1995, Elmegreen & Efremov 1997, Bastian & Goodwin 2006), i.e. at least an order of magnitude higher than SFEs in normal spiral and irregular galaxies, or in dwarf galaxy starbursts (cf. Krueger et al. 1995, Murgia et al. 2002). SFEs as high as 30 per cent or more, however, are observed in global and nuclear starbursts triggered by massive gas-rich mergers, such as NGC 7252, and ultra-luminous infrared galaxies (ULIRGs; Fritze-v. Alvensleben & Gerhard 1994, Gao & Solomon 2004) and led to the idea that GCs might form in these events and not only in the early Universe (Fritze-v. Alvensleben & Burkert 1995, Schweizer 2002, 2003).

In addition, observations of a gap in cluster ages but not in field star ages in the LMC (Rich et al. 2001) suggest that SC formation there took place in stages of enhanced star formation only, possibly related to close encounters of the LMC with the Milky Way and/or the SMC. Similarly, star cluster formation in M51 is found to have been significantly enhanced during the last close encounter with its companion NGC 5194 (Bastian et al. 005a), once again when the overall star formation and the SFE are expected to be enhanced.

Although little is known about molecular cloud *structures* in interacting and merging galaxies, a clear difference does exist in the molecular gas *content* between normal star-forming galaxies and ULIRGs. We know that while the CO(1-0) line traces molecular gas at densities $n \geqslant 100 \mathrm{cm}^{-3}$, the HCN(1-0) and CS (1-0) lines trace gas at densities $n \geqslant 10^4 \mathrm{cm}^{-3}$ and $n \geqslant 10^5 \mathrm{cm}^{-3}$, respectively.

Submillimetre observations show that for quiescently star-forming galaxies only a small fraction ($\sim 0.1 - 3$ per cent) of all their (CO) molecular gas is at the high densities of molecular cloud cores, as traced by HCN or CS, i.e. $L(\mathrm{HCN})/L(\mathrm{CO}) \sim 0.001 - 0.03$. In contrast, ULIRGs show

that, averaged over volumes of $(10 - 300 \text{ pc})^3$, the ratio $M(\text{HCN})/M(\text{CO})$ can reach up to $0.3 - 1$ (Gao & Solomon 2004), i.e. the molecular cloud structure must be very different from the case of quiescently star-forming galaxies – to the point that it becomes very difficult to imagine much internal structure at all, if essentially all the molecular gas is at molecular cloud core densities.

The mass ratio of high-density gas to the total gas mass (as traced by the $L(\text{HCN})/L(\text{CO})$ ratio) in ULIRGs is higher by a factor of $\sim 5 - 10$ when compared with normal star-forming galaxies (Gao & Solomon 2004). Since the mass in high-density gas correlates linearly with the star-formation rate (SFR; as measured by the far-infrared flux; Gao & Solomon 2004), ULIRGs therefore also possess a star formation per unit total gas mass higher by a factor $\sim 5 - 10$ compared to normal SF galaxies.

The Schmidt (1959) law relating the surface densities of the SFR and of hydrogen gas (H I from direct observations and H_2 as traced by CO) by $\Sigma_{\text{SFR}} \propto \Sigma_{\text{gas}}^n$ with $n \sim 1.4$ is valid from quiescently star-forming spirals all the way through to ULIRGs, probably the most actively star-forming galaxies in existence today (Kennicutt 1998), over almost 5 orders of magnitude in gas surface density and 6 orders of magnitude in SFR density. However, if this relation is expressed in terms of high-density gas, as traced by HCN or CS, instead of the low-density gas traced by CO, it becomes linear, indicating that star formation is more fundamentally governed by the content of *high density* gas, not the *overall* gas content (see Solomon et al. 1992, Gao & Solomon 2004). The non-linearity in the Kennicutt (1998) law might then arise from an environment-dependent time scale and/or efficiency to transform H I into H_2 and the low-density gas into high-density gas. This is an important issue to consider in hydrodynamical modelling of galaxies and galaxy mergers, which then needs to account for a multi-phase ISM and include a careful description of phase transitions, star formation and feedback processes.

Star formation in normal galaxies, spirals and irregulars, is thought to occur through the collapse of molecular clouds, whereby the mass spectrum apparently remains self-similar from molecular clouds through molecular cloud cores all the way to the mass spectrum of open star clusters, all of which are power laws with $m \sim -1.5$ to -2 (Lada & Lada 2003, see Elmegreen & Efremov 1997 for a theoretical foundation), implying a constant SFE. However, observations show considerable SFE scatter between different clouds and clusters (see e.g. Lada et al. 1997, Koo 1999, Lada & Lada 2003), although this quantity is naturally very difficult to measure. As the SFE is linked strongly non-linearly with the surviving bound fraction of the cluster (Lada et al. 1984, Geyer & Burkert 2001, Fellhauer & Kroupa 2005), deviations from this self-similarity are not coming as a surprise. Their impact on the form of the cluster LF (and MF) is studied extensively in Parmentier & Gilmore (2006), where it is shown to explain the occurrence of a turnover in the cluster LF derived from a power-law cloud LF (or MF). However, this whole issue is currently under vigorous debate (see also below).

In interacting galaxies, the frequency of molecular cloud collisions is expected to increase strongly and this will considerably enhance star formation. Moreover, molecular clouds get shock-compressed by external pressure (re-

cently verified observationally for the Antennae galaxies by Haas et al. 2005, although Whitmore et al. 2005 report the absence of shock-heated gas close to their sample of YSCs), grow denser and more massive, and this process can drive up the SFE very efficiently (Jog & Solomon 1992, Barnes 2004). Jog & Das (1992, 1996) have shown that a relatively small increase in the external ambient pressure to values 3 – 4 times the internal pressure within the molecular clouds in the undisturbed galaxy can drive SFEs up to 70 – 90 per cent.

5.3 Evolution of SC systems

Based on the observed power-law LFs of YSCs by van den Bergh & Lafontaine (1984) for the Milky Way and Hunter et al. (2003) for the LMC, a power-law LF is usually also adopted for YSC systems in interacting galaxies (see de Grijs et al. 003b for a recent compilation; also Zhang et al. 2001, Zepf et al. 1999, de Grijs et al. 2001), although in most cases these LFs cannot be traced to below the expected turnover magnitude, if there were one. In addition, in such violently star-forming systems the stellar contamination of the sample is more difficult to deal with, and the determination of observational completeness fractions is difficult because of strongly variable backgrounds. Non-negligible age differences among the YSCs lead to distortions of the LFs with respect to their underlying, intrinsic MFs (Meurer 1995, Fritze-v. Alvensleben 1999).

Approaching this issue from the opposite point of view, it is usually argued that the underlying MF is most likely a power-law, based on observations of the GMC MFs in nearby normal galaxies (e.g., Solomon et al. 1987, Elmegreen & Efremov 1997, Kramer et al. 1998, Zinchenko et al. 1998, Rosolowsky 2005, Rathborne et al. 2006). This argument has two drawbacks, however:

(i) It assumes that the cluster mass correlates directly with the mass of the precursor GMC, and hence must be subject to a constant SFE. As indirect measure, a correlation between mass and radius would then be expected. The presence of a mass-radius relation for GMCs and its absence for clusters (Ashman & Zepf 2001), however, casts doubt on the validity of this assumption. Present studies on these mass-radius relations are limited to nearby and therefore only relatively undisturbed galaxies, however. The impact of the observed cloud-cloud scatter in SFEs on the cluster LF/MF was recently studied by Parmentier & Gilmore (2006). Here, it was shown that this scatter can transform a power-law MF of GMCs into a bell-shaped star cluster MF.

(ii) It assumes that the GMC MFs in interacting galaxies are similar to those in nearby normal galaxies. However, as recently shown (Gao & Solomon 2004), of relevance for star formation is not the mass of the GMCs, but the mass of the dense cores embedded within these GMCs. The fraction of gas in these cores compared to the total gas mass is substantially higher in violently interacting and star-forming galaxies, compared to quiescently star-forming isolated galaxies (Gao & Solomon 2004). The MFs of both GMCs and of their cores in the nearest interacting and starburst galaxies, e.g. such as in the Antennae galaxies, will be determined

only to sufficiently low masses[7] when the next generation (sub)millimetre observatory ALMA becomes operational in the next decade. Until then, the initial cluster MF will likely be the best proxy, but see (i) above.

It has hitherto remained unclear whether the difference in shape between the power-law LFs of young SCs (but see Fritze-v. Alvensleben 1998, 1999, de Grijs et al. 003c and Goudfrooij et al. 2004 for the Gaussian LFs in the Antennae galaxies, M82B and NGC 1316, and the new results by de Grijs & Anders 2006 on the LMC SC system) and old GC systems is caused by differences in the nature and formation of the two types of clusters, or whether the power law of young systems is secularly transformed into the Gaussian distribution of old GC systems by selective destruction effects. Models for the evolution of SC systems in galactic potentials have naturally obtained a Gaussian shape from an initial power law by selectively destroying low-mass clusters (Fall & Zhang 2001). Detailed dynamical studies that also include dynamical friction as an important disruption mechanism for massive clusters (Vesperini 2000) show that although it is possible to obtain a final Gaussian distribution from an initial power-law, significant fine-tuning of the model parameters is required to obtain the observed GC mass function. In contrast, an initial Gaussian shape similar to that observed today is conserved for a wide range of assumptions despite the disruption of more than 50 per cent of the original cluster population. In addition, an initial Gaussian shape with parameters differing from the presently observed ones tend to evolve to a shape with the presently observed parameters at GC ages (Vesperini 2000). It is not yet possible to do this kind of modelling in the time-varying galactic potentials of merging galaxies. Parmentier & Gilmore (2005, 2006) have shown that the initial cluster MF of the Galactic GC system very probably was already either Gaussian in shape or described by a truncated power law with a cut-off at the same position as the turnover of the Gaussian distribution. Similarly, de Grijs et al. (2005) show that the *initial* cluster MF in the post-starburst region B in M82 (shown in de Grijs et al. 003c to possess a *present-day* cluster MF of roughly Gaussian shape) was also most likely of Gaussian shape, supported by plausibility arguments regarding the initial stellar density in this region.

5.4 Our results in this general framework

Our findings represent the youngest star cluster system for which a Gaussian-shaped LF fits statistically significantly better than a power-law distribution. This is an extension of the results found observationally by Goudfrooij et al. (2004) ($\simeq$ 3 Gyr-old cluster system in the merger remnant NGC 1316) and de Grijs et al. (003c) ($\simeq$ 1 Gyr-old cluster system in the fossil starburst region B in M82). It supports the detailed models by Vesperini (see Vesperini 2000 for a Gaussian initial LF and Vesperini

2001 for the power-law case), (Parmentier & Gilmore 2005, 2006) and de Grijs et al. (2005). In the framework of Parmentier & Gilmore (2006) the occurrence of the turnover at such early times is a natural outcome of shaping the LF during the earliest stages of cluster evolution, namely the phase of the removal of gas left over from cluster formation. Vesperini (2000) and de Grijs et al. (2005) show the necessity for an initial or very early Gaussian LF, which is in agreement with Parmentier & Gilmore (2006).

The proposed universality of the Gaussian *shape* of SC LFs, although not necessarily their (possibly environment-dependent) parameters, has far-reaching consequences for studies of star and star cluster formation. It opens the possibility to study the formation of massive bound clusters (proto-GCs) at close reach, a process that was previously thought to have taken place exclusively in the early Universe.

6   SUMMARY

In this paper we have studied the luminosity functions of the YSCs in the Antennae galaxies (NGC 4038/39), the nearest ongoing merger of two spiral galaxies. The merging process is accompanied by a strong burst of star formation, and particularly star cluster formation. We carefully select a sample of clearly extended sources, and hence remove the otherwise strong contamination by bright stars within the Antennae galaxies.

The complex background, caused by the interaction and the contamination by bright stars, hampers the accurate determination of the observational completeness. However, an accurately determined completeness function is essential to determine whether or not the intrinsic LF of the cluster system shows a turnover like the old GC systems. We present a number of tests on the completeness functions, and showed that it is essential to include *all* cluster selection criteria in the determination of the completeness function.

We attempted to fit the intrinsic LFs with the most widely used models, i.e. a power-law distribution and a Gaussian distribution, taking the completeness function and the photometric errors into account. We find statistically significant evidence that the LFs of this sample of clearly extended sources are best described by an intrinsic Gaussian distribution. We determine the chance of error (i.e. the probability that we erroneously discard a better-fitting power-law distribution) using Monte Carlo-simulations, and find it to be below 0.5 per cent.

Earlier claims of power-law LFs suffer most likely from the strong stellar contamination and the difficulties in the completeness determination. In addition, the statistical tools developed for this study are beyond the sensitivity of any commonly used tools.

---

[7] Following Wilson et al. (2003) and the ALMA sensitivity calculator (http://www.eso.org/projects/alma/science/bin/sensitivity.html), we roughly estimate limiting GMC masses to be observed in the Antennae galaxies by ALMA around 6×10^4 M$_\odot$ (1 hr observation) to 1×10^4 M$_\odot$ (30 hr observation).

REFERENCES

Anders P., Bissantz N., Fritze-v. Alvensleben U., de Grijs R., 2004a, MNRAS, 347, 196

Anders P., de Grijs R., Fritze-v. Alvensleben U., Bissantz N., 2004b, MNRAS, 347, 17

Anders P., Fritze-v. Alvensleben U., 2003, A&A, 401, 1063

Anders P., Gieles M., de Grijs R., 2006, A&A, 451, 375

Ashman K. M., Conti A., Zepf S. E., 1995, AJ, 110, 1164

Ashman K. M., Zepf S. E., 1998, Globular Cluster Systems. Cambridge astrophysics series ; 30, Cambridge University Press, Cambridge, U. K. ; New York

Ashman K. M., Zepf S. E., 2001, AJ, 122, 1888

Barnes J. E., 1988, ApJ, 331, 699

Barnes J. E., 2004, MNRAS, 350, 798

Bastian N., Emsellem E., Kissler-Patig M., Maraston C., 2006, A&A, 445, 471

Bastian N., Gieles M., Efremov Y. N., Lamers H. J. G. L. M., 2005b, A&A, 443, 79

Bastian N., Gieles M., Lamers H. J. G. L. M., Scheepmaker R. A., de Grijs R., 2005a, A&A, 431, 905

Bastian N., Goodwin S. P., 2006, MNRAS, 369, L9

Brown J. H., Burkert A., Truran J. W., 1995, ApJ, 440, 666

Bruzual G., Charlot S., 2003, MNRAS, 344, 1000

Cresci G., Vanzi L., Sauvage M., 2005, A&A, 433, 447

de Grijs R., Anders P., 2006, MNRAS, 366, 295

de Grijs R., Anders P., Bastian N., Lynds R., Lamers H. J. G. L. M., O'Neil E. J., 2003b, MNRAS, 343, 1285

de Grijs R., Bastian N., Lamers H. J. G. L. M., 2003c, ApJ, 583, L17

de Grijs R., Lee J. T., Clemencia Mora Herrera M., Fritze-v. Alvensleben U., Anders P., 2003a, New Astronomy, 8, 155

de Grijs R., O'Connell R. W., Gallagher III J. S., 2001, AJ, 121, 768

de Grijs R., Parmentier G., 2007, submitted to ChJA&A

de Grijs R., Parmentier G., Lamers H. J. G. L. M., 2005, MNRAS, 364, 1054

Elmegreen B. G., Efremov Y. N., 1997, ApJ, 480, 235

Elson R. A. W., Fall S. M., 1985, PASP, 97, 692

Elson R. A. W., Fall S. M., Freeman K. C., 1987, ApJ, 323, 54

Fabbiano G., Krauss M., Zezas A., Rots A., Neff S., 2003, ApJ, 598, 272

Fall S. M., Chandar R., Whitmore B. C., 2005, ApJ, 631, L133

Fall S. M., Zhang Q., 2001, ApJ, 561, 751

Fellhauer M., Kroupa P., 2005, ApJ, 630, 879

Forbes D. A., 1996, AJ, 112, 954

Fritze-v. Alvensleben U., 1998, A&A, 336, 83

Fritze-v. Alvensleben U., 1999, A&A, 342, L25

Fritze-v. Alvensleben U., 2004, A&A, 414, 515

Fritze-v. Alvensleben U., Burkert A., 1995, A&A, 300, 58

Fritze-v. Alvensleben U., Gerhard O. E., 1994, A&A, 285, 775

Gao Y., Solomon P. M., 2004, ApJ, 606, 271

Geyer M. P., Burkert A., 2001, MNRAS, 323, 988

Gieles M., Larsen S. S., Scheepmaker R. A., Bastian N., Haas M. R., Lamers H. J. G. L. M., 2006, A&A, 446, L9

Goodwin S. P., Bastian N., 2006, MNRAS, 373, 752

Goudfrooij P., Gilmore D., Whitmore B. C., Schweizer F., 2004, ApJ, 613, L121

Haas M., Chini R., Klaas U., 2005, A&A, 433, L17

Harris W. E., 1991, ARA&A, 29, 543

Hibbard J. E., et al. 2005, ApJ, 619, L87

Hibbard J. E., van der Hulst J. M., Barnes J. E., Rich R. M., 2001, AJ, 122, 2969

Hunter D. A., Elmegreen B. G., Dupuy T. J., Mortonson M., 2003, AJ, 126, 1836

Jog C. J., Das M., 1992, ApJ, 400, 476

Jog C. J., Das M., 1996, ApJ, 473, 797

Jog C. J., Solomon P. M., 1992, ApJ, 387, 152

Kassin S. A., Frogel J. A., Pogge R. W., Tiede G. P., Sellgren K., 2003, AJ, 126, 1276

Kavelaars J. J., Harris W. E., Hanes D. A., Hesser J. E., Pritchet C. J., 2000, ApJ, 533, 125

Kennicutt Jr. R. C., 1998, ApJ, 498, 541

King I., 1962, AJ, 67, 471

Knierman K. A., Gallagher S. C., Charlton J. C., Hunsberger S. D., Whitmore B., Kundu A., Hibbard J. E., Zaritsky D., 2003, AJ, 126, 1227

Koo B.-C., 1999, ApJ, 518, 760

Kramer C., Stutzki J., Rohrig R., Corneliussen U., 1998, A&A, 329, 249

Krist J., Hook R., 2004, The Tiny Tim User's Guide. STScI, Baltimore, 6.3 edn

Krueger H., Fritze-v. Alvensleben U., Loose H.-H., 1995, A&A, 303, 41

Lada C. J., Lada E. A., 2003, ARA&A, 41, 57

Lada C. J., Margulis M., Dearborn D., 1984, ApJ, 285, 141

Lada E. A., Evans II N. J., Falgarone E., 1997, ApJ, 488, 286

Larsen S. S., 1999, A&AS, 139, 393

Larsen S. S., 2004, A&A, 416, 537

Larsen S. S., Brodie J. P., Hunter D. A., 2004, AJ, 128, 2295

Lehmann E. L., 1994, Testing statistical hypotheses. Chapman & Hall, New York

Little R. J. A., Rubin D. B., 2002, Statistical analysis with missing data, second edn. Wiley Series in Probability and Statistics, Wiley-Interscience [John Wiley & Sons], Hoboken, NJ

McLaughlin D. E., Pudritz R. E., 1996, ApJ, 457, 578

Mengel S., Lehnert M. D., Thatte N., Genzel R., 2005, A&A, 443, 41

Metz J. M., Cooper R. L., Guerrero M. A., Chu Y.-H., Chen C.-H. R., Gruendl R. A., 2004, ApJ, 605, 725

Meurer G. R., 1995, Nature, 375, 742

Mirabel I. F., Vigroux L., Charmandaris V., Sauvage M., Gallais P., Tran D., Cesarsky C., Madden S. C., Duc P.-A., 1998, A&A, 333, L1

Murgia M., Crapsi A., Moscadelli L., Gregorini L., 2002, A&A, 385, 412

Neff S. G., Ulvestad J. S., 2000, AJ, 120, 670

Parmentier G., Gilmore G., 2005, MNRAS, 363, 326

Parmentier G., Gilmore G., 2006, submitted to MNRAS

Patil G. P., Rao C. R., 1978, Biometrics, 34, 179

Rathborne J. M., Jackson J. M., Simon R., 2006, ApJ, 641, 389

Rich R. M., Shara M. M., Zurek D., 2001, AJ, 122, 842

Rosolowsky E., 2005, PASP, 117, 1403

Sandage A., Tammann G. A., 1995, ApJ, 446, 1

Saviane I., Hibbard J. E., Rich R. M., 2004, AJ, 127, 660

Schlegel D. J., Finkbeiner D. P., Davis M., 1998, ApJ, 500, 525

Schmidt M., 1959, ApJ, 129, 243

Schulz J., Fritze-v. Alvensleben U., Möller C. S., Fricke K. J., 2002, A&A, 392, 1

Schweizer F., 2002, in Geisler D., Grebel E. K., Minniti D., eds, IAU Symposium Evolution of Globular Clusters Formed in Mergers. p. 630

Schweizer F., 2003, Dynamics and Evolution of Dense Stellar Systems, 25th meeting of the IAU, Joint Discussion 11, 18 July 2003, Sydney, Australia, 11

Schweizer F., Seitzer P., 1998, AJ, 116, 2206

Solomon P. M., Downes D., Radford S. J. E., 1992, ApJ, 387, L55

Solomon P. M., Rivolo A. R., Barrett J., Yahil A., 1987, ApJ, 319, 730

van den Bergh S., Lafontaine A., 1984, AJ, 89, 1822

Vesperini E., 2000, MNRAS, 318, 841

Vesperini E., 2001, MNRAS, 322, 247

Wang Z., Fazio G. G., Ashby M. L. N., Huang J.-S., Pahre M. A., Smith H. A., Willner S. P., Forrest W. J., Pipher J. L., Surace J. A., 2004, ApJS, 154, 193

West M. J., Côté P., Marzke R. O., Jordán A., 2004, Nature, 427, 31

Whitmore B. C., 2004, in Lamers H. J. G. L. M., Smith L. J., Nota A., eds, ASP Conf. Ser. 322: The Formation and Evolution of Massive Young Star Clusters Survival Rates and Consequences. pp 419–+

Whitmore B. C., Chandar R., Fall S. M., 2006, ArXiv Astrophysics e-prints

Whitmore B. C., Gilmore D., Leitherer C., Fall S. M., Chandar R., Blair W. P., Schweizer F., Zhang Q., Miller B. W., 2005, AJ, 130, 2104

Whitmore B. C., Schweizer F., 1995, AJ, 109, 960

Whitmore B. C., Schweizer F., Leitherer C., Borne K., Robert C., 1993, AJ, 106, 1354

Whitmore B. C., Zhang Q., 2002, AJ, 124, 1418

Whitmore B. C., Zhang Q., Leitherer C., Fall S. M., Schweizer F., Miller B. W., 1999, AJ, 118, 1551

Wilson C. D., Scoville N., Madden S. C., Charmandaris V., 2003, ApJ, 599, 1049

Zepf S. E., Ashman K. M., English J., Freeman K. C., Sharples R. M., 1999, AJ, 118, 752

Zhang Q., Fall S. M., 1999, ApJ, 527, L81

Zhang Q., Fall S. M., Whitmore B. C., 2001, ApJ, 561, 727

Zinchenko I., Pirogov L., Toriseva M., 1998, A&AS, 133, 337